Thin Solid Films 535 (2013) 22–26

Contents lists available at SciVerse ScienceDirect

Thin Solid Films

journal homepage: www.elsevier.com/locate/tsf

Annealing behavior of reactively sputtered precursor films for Cu_2ZnSnS_4 solar cells

Tove Ericson *, Jonathan J. Scragg, Tomas Kubart, Tobias Törndahl, Charlotte Platzer-Björkman

Ångström Solar Center, Solid State Electronics, Uppsala University, Box 534, SE-75121 Uppsala, Sweden

ARTICLE INFO

Available online 29 October 2012

Keywords:
Cu_2ZnSnS_4
CZTS
Kesterite
Reactive sputtering
Thin film solar cell
Stress
Density

ABSTRACT

Reactively sputtered Cu–Zn–Sn–S precursor films are prepared and recrystallized by rapid thermal processing to generate Cu_2ZnSnS_4 solar cell absorber layers. We study how the film properties are affected by substrate heating and composition. The stress, density and texture in the films were measured. Compressive stress was observed for the precursors but did not correlate to the deposition temperature, and had no influence on the properties of the annealed films or solar cells. However, the substrate temperature during precursor deposition had a large effect on the behavior during annealing and on the solar cell performance. The films deposited at room temperature had, after annealing, smaller grains and cracks, and gave shunted devices. Cracking is suggested to be due to a slightly higher sulfur content, lower density or to minor differences in material quality. The grain size in the annealed films seems to increase with higher copper content and higher precursor deposition temperature. The best device in the current series gave an efficiency of 4.5%.

1. Introduction

The quaternary semiconductor $Cu_2ZnSn(S,Se)_4$ (CZTSSe) is interesting as an In-free replacement for $Cu(In,Ga)Se_2$ (CIGS). The current world record of over 10% [1] is encouraging for further improvements. The most successful fabrication process so far is the two step method containing a deposition step, which gives a homogeneous precursor film with full chalcogen content, and then a short anneal to allow the film to crystallize into CZTSSe [1]. It is suggested that this is because CZTSSe risks decomposing when high temperatures are combined with low pressures [2], meaning that it is not well-suited for single-step vacuum deposition at high temperature, the typical approach for CIGS.

In this work we produce Cu_2ZnSnS_4 (CZTS) precursors using reactive co-sputtering of Cu, Zn and Sn in an H_2S atmosphere, giving films which are homogeneous and have a tuneable composition. A rapid anneal of the precursor then creates a large grained film suitable for solar cells.

Previously only a few publications describe reactively sputtered CZTS. In 2010, Liu et al. studied the properties of their dense reactively sputtered CZTS films [3] and the same year Chawla et al. produced reactively sputtered CZTS solar cells in a one step process and achieved an efficiency of 1.35% [4]. Grain boundary properties of 3.37% efficient, reactively sputtered and annealed CZTS were investigated in [5].

In [6] we described a precursor series with different substrate heating during deposition. However, since the other settings in this series were kept constant, the composition varied significantly between the samples. To be able to differentiate the effect of composition from the effect of heating, we here investigate samples with three different compositions for every deposition temperature. We also investigate the connection between the precursor deposition parameters and the annealed film properties and the final solar cell performance.

2. Experimental details

Film depositions were performed using Zn and Cu:Sn alloy targets as described in detail in [6]. Two different CuSn-targets were used, one with composition Cu: 62.5 at.% and Sn: 37.5 at.% (purity 99.99%) and one with Cu: 65 at.% and Sn: 35 at.% (purity 99.999%). Both targets were operated in constant power mode with powers in the range of 520–570 W for the CuSn-target and 550–680 W for the Zn-target. H_2S with a purity of 99.5% was supplied at a mass flow rate of 30 sccm, giving a constant pressure of 0.67 Pa. The setting for the radiative front side heater was either off, 300 °C or 500 °C, yielding temperatures at the substrate of approximately 40 °C, 180 °C and 300 °C respectively. The sputtering time was 40–80 min giving thicknesses around 2 μm. The precursors were annealed in a tube furnace under a static argon atmosphere (35 kPa) at 560 °C for 3 min as described in detail in [7].

Four different substrates were used for depositions: glass for profilometer thickness measurements, silicon wafer for sulfur content measurement, Mo-coated glass for other characterization techniques and solar cell fabrication and a thin (100 μm) Mo-coated glass (cover glass D 263® M from Schott) for stress measurements. The stress was measured with a Veeco Dektak 150 profilometer as described in detail in [6]. The density of the precursors was calculated from the metal atom amount from x-ray fluorescence (XRF) measurement, using a Rutherford backscattering (RBS) calibration, together with the energy

* Corresponding author. Tel.: +46 18 4717255; fax: +46 18 555095.
E-mail address: tove.ericson@angstrom.uu.se (T. Ericson).

0040-6090/$ – see front matter
http://dx.doi.org/10.1016/j.tsf.2012.10.081

dispersive spectroscopy (EDS) measurement of sulfur content and the thickness measured with the profilometer. For the annealed films it was assumed that the sulfur content was stoichiometric.

The metal composition of the films was determined by XRF in a PANalytical Epsilon 5. The XRF counts were correlated to metal composition via a thickness series measured by RBS, for details see [6]. The sulfur content of the films was measured with EDS at 20 keV, in a LEO 440 scanning electron microscopy (SEM) with an EDAX system.

Thickness measurements were made with a Veeco Dektak 150 profilometer. A LEO 1550 SEM at 5 keV was used to investigate the morphology of both precursor and annealed films.

A Siemens D5000 in Bragg-Brentano focusing geometry was used for θ–2θ x-ray diffraction (XRD). For residual stress and pole figure measurements, a Philips X'pert MRD diffractometer, point focus set-up, with a polycapillary X-ray lens on the primary side and a parallel plate collimator (0.18°) with flat graphite monochromator on the detector side, was used. For all XRD techniques the radiation was CuK_{α}. Raman scattering was measured with a Renishaw system at an excitation wavelength of 514 nm. Device finishing and characterization are described in [7].

Nine samples with varying composition and different substrate heating during deposition, according to Table 1, were prepared. The Zn content was kept between $Zn/(Cu+Sn) = 0.36–0.41$.

3. Results and discussion

First, we discuss the as-deposited precursors, defined in Table 1. From SEM cross sections (Fig. 1) it is seen that the precursors are generally dense with a columnar structure. The low temperature depositions exhibit features of zone 1–zone T of the structure zone model (SZM) [8] with narrow columns and rounded surfaces. The high temperature deposition appearance is closer to zone T–zone 2 morphology, exhibiting a facetted surface and angled grain boundaries within the film. These observations match well with the predictions of the SZM.

Precursor properties are given in Table 2. As seen in our earlier study [6], the sulfur content is slightly over-stoichiometric for the low temperature depositions and decreases for the high temperature films, probably due to the high vapor pressure of S_2. The density is also slightly lower for the films deposited at room temperature. Sample C3 (SEM not shown), which was the most copper rich sample, had a more granular, porous morphology, and accordingly gives a low calculated density.

θ–2θ XRD scans of the precursors (Fig. 2) show broad peaks which match a cubic structure, like that of ZnS [9]. There are also additional peaks from the back contact, Mo [10]. The relative peak intensities deviate from the powder reference of ZnS (and CZTS) in a way which indicates that the films have a (111) orientation with the close packed plane parallel to the surface (corresponding to (112) orientation for CZTS). The degree of texture increases with higher deposition temperature and the highest temperature diffractogram is clearly dominated by the texture peaks. A (200) pole figure (not shown) was recorded on the C2 sample and this confirms that the film has a (111) preferred orientation and also shows that no in-plane orientation exists.

Table 1
Samples described in this study, grouped by Cu/Sn ratio and deposition temperature.

	Cu/Sn		
Estimated substrate temperature during precursor deposition [°C]	1.69–1.85	1.95–1.99	2.04–2.16
40	A1[a]	A2[b]	A3[b]
180	B1[a]	B2[b]	B3[b]
300	C1[a]	C2[a]	C3[b]

[a] Precursors deposited from target with composition Cu: 62.5 at.% and Sn: 37.5 at.%.
[b] Precursors deposited from target with composition Cu: 65 at.% and Sn: 35 at.%.

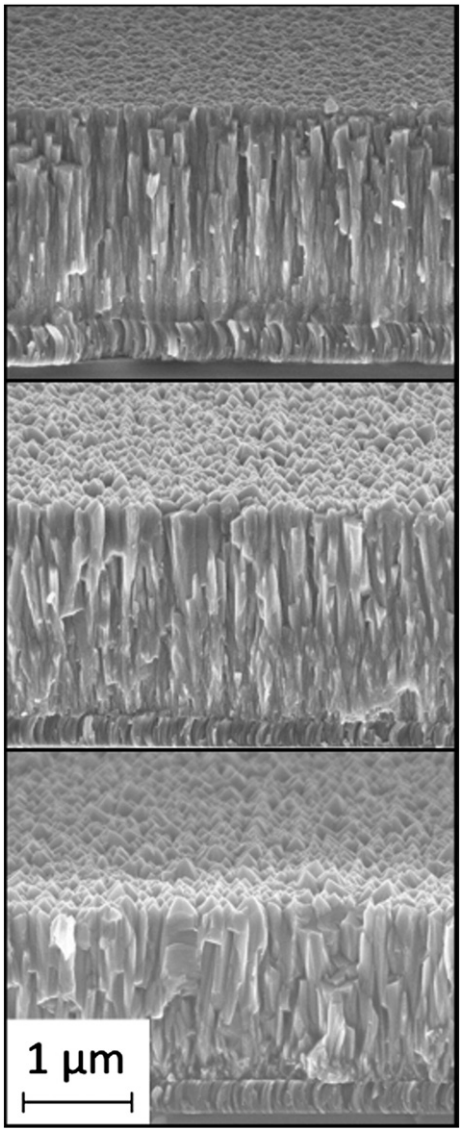

Fig. 1. SEM images of precursors for the three different deposition temperatures. From top to bottom: A2 (40 °C), B2 (180 °C), and C2 (300 °C). The precursor surface is increasingly facetted as the temperature is raised.

Raman scattering measurements of the precursors show a clear but broad peak at 330–336 cm^{-1} (Fig. 3). The peak is more defined for the higher temperature samples. Peak fitting with Lorentzian curves indicates three weaker contributions encompassed in the broad peak, at 251–255, 288–291 and 354–360 cm^{-1}. These peak positions match quite well the response expected from CZTS [11,12]. Sample C3 also shows a small peak at 475 cm^{-1} which could originate from CuS [13] since this sample has the highest Cu-content. The XRD and Raman results, together with the homogenous precursor appearance in SEM, makes us suggest that the reactively sputtered precursors have a non-equilibrium structure, with the sulfur ions in the cubic zinc-blende configuration and the metal ions randomly ordered at the cation sites; this is more thoroughly discussed in [7].

Stress measurement from deflection of thin glass substrates (Table 2) show compressive stress for all samples except for C3, which, as noted, has a different morphology. No trend in the stress values with deposition temperature can be seen. Differences in stress values can also give rise to peak shifts in θ–2θ XRD, although several other factors, such as composition, could also have an influence. In this series, the shift of the most

Table 2
Properties of precursor and corresponding annealed films. After annealing the 2θ XRD value for the (112) peak was generally just below 28.5°, close to the CZTS powder reference value 28.4502°[14].

	Precursor					Annealed		
Sample	S/metals	Thickness [nm]	Calc. density [g/cm^2]	Avg. stress [MPa]	(111)/(112) 2θ from XRD [°]	Thickness [nm]	Calc. density [g/cm^2]	Anneal/etch behavior
A1	1.15	2080	3.82	−143	28.306	1990	3.89	Cracked/peeled off
A2	1.03	2020	3.99	−4	28.319	1940	4.04	Cracked/OK
A3	1.05	1890	3.95	−18	28.313	1880	3.97	Cracked/OK
B1	1.03	1950	4.08	−183	28.294	1900	4.19	OK/OK
B2	0.97	2040	4.10	−75	28.342	2040	4.19	OK/OK
B3	0.96	2020	4.16	−43	28.356	2080	N/A	OK/OK
C1	0.99	1970	3.98	−161	28.298	1920	4.22	OK/OK
C2	1.00	1860	4.06	−120	28.323	1850	4.20	OK/OK
C3	0.94	2080	3.54	34	28.412	2020	3.64	Porous/partly peeled off

intense peak from the position expected for ZnS or CZTS (28.531° and 28.4502° respectively [9,14]), does follow the stress within each temperature group (Table 2). Using XRD for residual stress measurements on a sample which had a high stress and had a weak preferred orientation (the room temperature sample from our previous series [6]) showed good agreement with the corresponding curvature measurement. But when using the same method on the higher temperature samples in this series it was apparent that the texture of the film made the XRD measurement uncertain. However, it was possible to confirm the stress trends seen from the other methods.

After annealing, the morphology is drastically changed. True for all samples is that the grains have grown substantially and that no columnar structure is left (Fig. 4). All films also contain small, bright grains, which we with EDS mapping in transmission electron microscope have observed to be ZnS. The samples deposited at room temperature have 100–200 nm wide, vertical cracks dividing the film into islands on the 10 μm scale. The grain size after annealing seems to increase both with precursor deposition temperature and increasing copper content, and is possibly inhibited by over-stoichiometric sulfur content in the precursors. The density of the films generally increases slightly during annealing, assuming that the sulfur content is stoichiometric in the annealed films. The thickness and the metal composition do not change significantly after the annealing.

In θ–2θ XRD, several more peaks appear and the pattern fits well to CZTS [14] with additional peaks for the Mo back contact, as before (Fig. 2). No unidentified peaks were seen. The peak shift from the reference pattern is significantly smaller than for the precursors, the main peak being around 28.5°, indicating that the stress has relaxed during annealing. The relative peak intensities are closer to the powder reference, although do not match perfectly. The difference is largest for the high temperature deposition, suggesting that some of the texture of the precursor could remain after annealing.

Raman scattering from the annealed samples shows a strong peak at 335–338 cm^{-1} and weaker contributions at 164, 250–252, 285–288, 348–350 and 363–372 cm^{-1} (Fig. 3). All peaks can be explained by the presence of CZTS [11,12]. The 348–350 cm^{-1} peak fits also with the main mode of ZnS [15] which would agree with the samples being slightly Zn-rich. Cu_2SnS_3 [16,17] should also have Raman intensity at this position and is another possible match. No correlation between the shape of the spectrum and substrate temperature or composition was observed.

Processing the annealed samples into solar cells caused the film of A1 to peel off completely. The other two samples from precursors deposited at room temperature were mostly shunted; there was only one working cell in A2 and none in A3. The C3 sample partly peeled off but the device from the remaining material actually gave the highest efficiency in this series at 4.5% (V_{oc}: 0.62 V, J_{sc}: 11.8 mA, FF: 63%). The current–voltage curve for this sample is shown in Fig. 5. For the other samples, the solar cell parameters are lower but quite even, with the exception of some slightly shunted cells. The cells are limited in all parameters and the best cell from each sample had device parameters of V_{oc} between 0.48–0.56 V, J_{sc} between 8.8–12.2 mA and fill factors in the range of 41–55% giving efficiencies of 2.5–3%. A more thorough evaluation of the solar cell performance of a similar device is given in [7].

It was expected that the sputter parameters for the precursors would influence the final properties of the annealed films and solar cells. In our previous study, we observed higher stresses in lower temperature depositions [6]. Annealing these same films resulted in

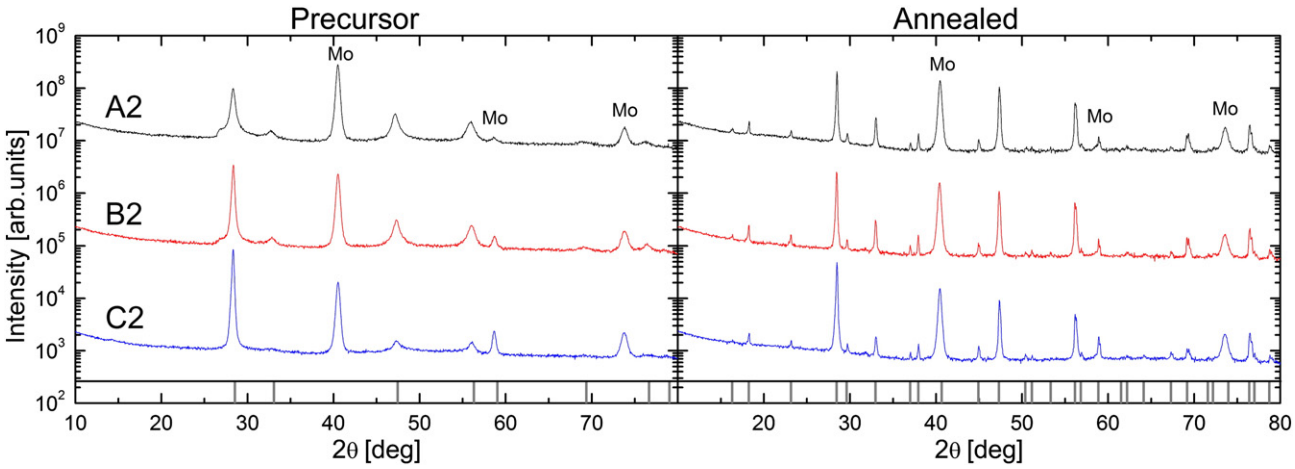

Fig. 2. θ–2θ-XRD on samples A2, B2 and C2 before and after annealing. Precursors show broad peaks best matching a cubic structure, like that of ZnS [9] (also indicated in the bottom of the left graph). The relative peak heights indicate a (111) orientation and that the texture increases with higher deposition temperature. The annealed samples show peaks matching well with CZTS [14] (indicated in the bottom of the right graph). The relative peak intensities are close to the powder reference, although do not match perfectly, suggesting that some of the texture from the precursors could be left. Peaks from the Mo back contact ([10], marked as "Mo" in the figure) can be seen in all diffractograms.

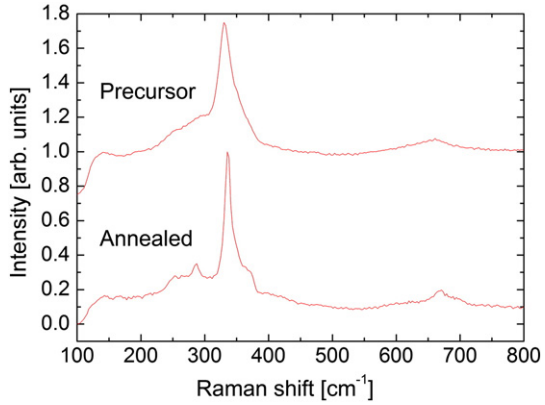

Fig. 3. Raman spectra (from sample B2) before and after the anneal. The precursor shows a clear but broad peak at 331 cm^{-1} with weak contributions at 254, 288 and 354 cm^{-1}. No trend was seen comparing different compositions but increased deposition temperature gave a more defined peak. The annealed sample shows a strong peak at 336 cm^{-1} and weaker contributions at 164, 252, 286, 350, 363 and 372 cm^{-1}. The intensity and position of these contributions varied slightly between the samples in the series but no trends with composition or deposition temperature were observed.

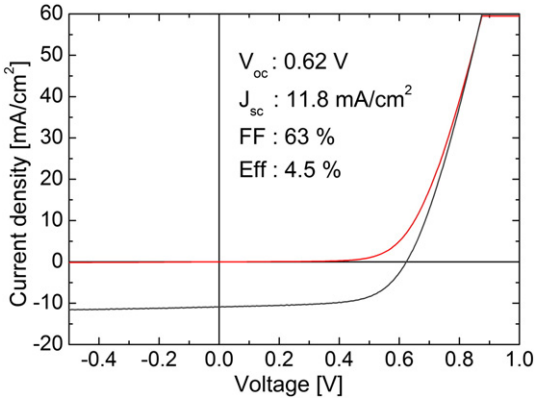

Fig. 5. Current–voltage curve and solar cell parameters for the sample with the highest efficiency (C3).

cracking, which we attributed to the high stress. However, in that series the composition changed together with the deposition temperature, with higher copper content in the high temperature depositions. In

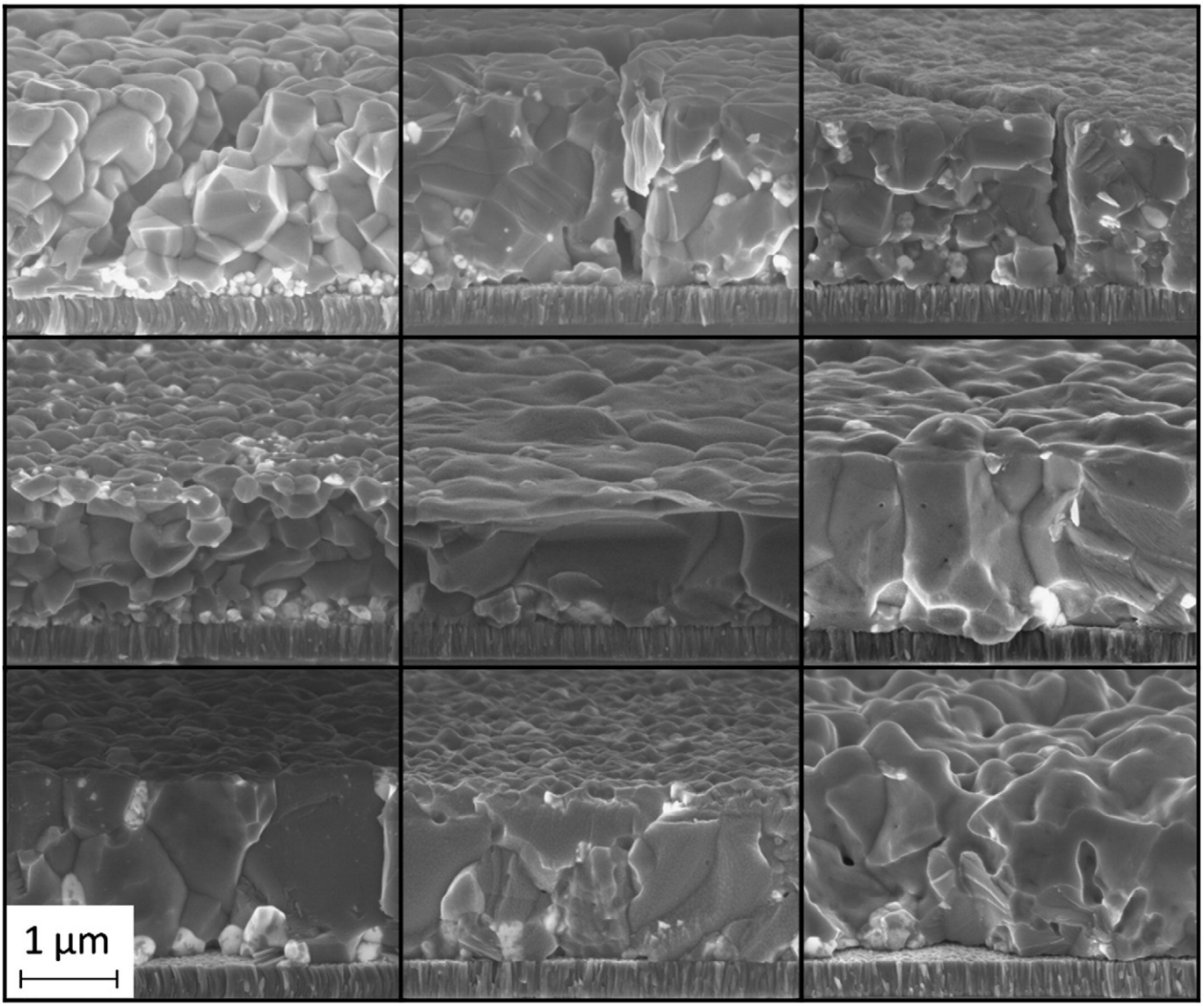

Fig. 4. SEM images of the annealed samples. Top row: precursors A1–A3 deposited at room temperature; middle row: precursors B1–B3 deposited at 180 °C; bottom row: precursors C1–C3 deposited at 300 °C. The copper content of the films increases going from left to right (see Table 1). 100–200 nm cracks are observed in the room temperature samples. The small, brighter grains seen in the films are observed to be ZnS. Sample B2 appears thinner in the image due to charging effects.

the current series, where the composition was controlled, no correlation between the deposition temperature and the amount of stress was seen. However, there is a slight correlation between high copper content and lower stress and this would also agree with our previous study. A further possible explanation for the stress variations is that the copper rich samples were made with a different sputtering target (see Table 1) and at a higher deposition rate, which theoretically should increase compressive stress [18], the opposite to what is seen here. Additionally, direct comparisons of stress levels in films deposited from different targets is not straightforward, since the angular distribution of the energetic species changes with the evolution of the racetrack, resulting in different growth conditions. Interestingly, the stress value does not seem to affect the morphology of the annealed films or the performance of the solar cells. For example, cracking was seen in all samples annealed from precursors deposited at room temperature despite the initial spread in stress.

Instead of stress, it appears that what differentiates the precursors deposited at room temperature is a slightly lower density, slightly higher sulfur content and a minor difference in texture and crystallinity, judging from θ–2θ XRD and Raman scattering. From this study we cannot conclude if the low density and the higher sulfur content are connected or if the low density originates from a porous morphology. Either could however be a plausible explanation for the annealing behavior. The loss of excess sulfur or elimination of porosity could both lead to the formation of cracks in the annealing process. The generally low density of the precursors, compared to the calculated value for CZTS (4.58 g/cm^3 derived from [19]), is not surprising in films that are sputtered at low temperature [18]. For the annealed films a lower density than the bulk value is most likely due to voids.

The trend in grain size with precursor deposition temperature in the annealed films could indicate that the atomic structure of the heated precursors is more similar to that of CZTS, and therefore that larger grains can form during the same annealing time. However, another parameter changing with the deposition temperature in this series is the sulfur content. A larger grain size with increasing copper content is well known for CIGS [20] and has also been reported for CZTS [21].

4. Conclusions

Reactively sputtered Cu–Zn–Sn–S precursors were prepared and recrystallized by rapid thermal processing to generate CZTS films. The influence of substrate heating and composition was studied. The substrate temperature during precursor deposition had a pronounced influence on the resulting annealed film and solar cell properties. The annealed films from precursors sputtered at room temperature had cracks and smaller grains, and the resulting devices were shunted. This could be due to the slightly higher sulfur content, lower density or minor differences in texture and crystallinity. Stress in the precursors, however, does not seem to affect film or solar cell properties.

Precursors made with a higher copper content and at higher precursor deposition temperatures gave generally larger grains, although no direct correlation with the device parameters was seen.

The best solar cell from this series gave an efficiency of 4.5% (V_{oc}: 0.62 V, J_{sc}: 11.8 mA, FF: 63%).

Acknowledgments

The authors acknowledge the financial support from the Swedish Energy Agency, Vinnova through the Vinnmer program, the Göran Gustafsson Foundation and the Carl Trygger Foundation.

References

[1] D.A. Barkhouse, O. Gunawan, T. Gokmen, T. Todorov, D. Mitzi, Prog. Photovoltaics 20 (1) (2012) 6.
[2] J.J. Scragg, T. Ericson, T. Kubart, M. Edoff, C. Platzer-Björkman, Chem. Mater. 23 (20) (2011) 4625.
[3] F.Y. Liu, K. Zhang, Y.Q. Lai, J. Li, Z.A. Zhang, Y.X. Liu, Electrochem. Solid-State Lett. 13 (11) (2010) H379.
[4] V. Chawla, B. Clemens, in: IEEE Phot. Spec. Conf. 35th, 2010, p. 1902.
[5] J.B. Li, V. Chawla, B.M. Clemens, Adv. Mater. 24 (6) (2012) 720.
[6] T. Ericson, T. Kubart, J.J. Scragg, C. Platzer-Björkman, Thin Solid Films 520 (24) (2012) 7093.
[7] J.J. Scragg, T. Ericson, X. Fontané, V. Izquierdo-Roca, A. Pérez-Rodríguez, T. Kubart, M. Edoff, C. Platzer-Björkman, Prog. Photovoltaics (2012), http://dx.doi.org/10.1002/pip.2265.
[8] J.A. Thornton, J. Vac. Sci. Technol. 11 (4) (1974) 666.
[9] E.A. Jumpertz, Z. Elektrochem. 59 (5) (1955) 419.
[10] H.E. Swanson, E. Tatge, in: Natl. Bur. Stand. (U.S.), Circ., 539/1, 1953, p. 20.
[11] M. Altosaar, J. Raudoja, K. Timmo, M. Danilson, M. Grossberg, J. Krustok, E. Mellikov, Phys. Status Solidi A 205 (1) (2008) 167.
[12] M. Himmrich, H. Haeuseler, Spectrochim. Acta, Part A 47 (7) (1991) 933.
[13] C.G. Munce, G.K. Parker, S.A. Holt, G.A. Hope, Colloids Surf., A 295 (1-3) (2007) 152.
[14] S. Schorr, H.J. Hoebler, M. Tovar, Eur. J. Mineral. 19 (1) (2007) 65.
[15] W.G. Nilsen, Phys. Rev. 182 (3) (1969) 838.
[16] P.A. Fernandes, P.M.P. Salome, A.F. da Cunha, J. Alloys Compd. 509 (28) (2011) 7600.
[17] D.M. Berg, R. Djemour, L. Gutay, S. Siebentritt, P.J. Dale, X. Fontane, V. Izquierdo-Roca, A. Perez-Rodriguez, Appl. Phys. Lett. 100 (19) (2012), http://dx.doi.org/10.1063/1.4712623.
[18] J.A. Thornton, D.W. Hoffman, Thin Solid Films 171 (1) (1989) 5.
[19] S. Siebentritt, S. Schorr, Prog. Photovoltaics 20 (5) (2012) 512.
[20] R.A. Mickelsen, W.S. Chen, Y.R. Hsiao, V.E. Lowe, IEEE Trans. Electron Devices 31 (5) (1984) 542.
[21] T. Tanaka, A. Yoshida, D. Saiki, K. Saito, Q. Guo, M. Nishio, T. Yamaguchi, Thin Solid Films 518 (2010) 29.